2021

Non-Equilibrium Behavior of Large-Scale Axial Vortex Cores

Robert L. Ash
Old Dominion University

Irfan R. Zardadkhan

Original Publication Citation

Ash, R. L., & Zardadkhan, I. R. (2021). Non-equilibrium behavior of large-scale axial vortex cores. *AIP Advances, 11*(2), 6 pp., Article 025320. https://doi.org/10.1063/5.0031668

Non-equilibrium behavior of large-scale axial vortex cores

Cite as: AIP Advances 11, 025320 (2021); doi: 10.1063/5.0031668
Submitted: 12 October 2020 • Accepted: 16 January 2021 •
Published Online: 11 February 2021

Robert L. Ash[1,a] and Irfan R. Zardadkhan[2,b]

AFFILIATIONS

[1]Mechanical and Aerospace Engineering Department, Old Dominion University, Norfolk, Virginia 23529, USA
[2]Tigercat Industries, Inc., Paris, Ontario N3L 3T6, Canada

[a]Author to whom correspondence should be addressed: rash@odu.edu
[b]Electronic address: irfan76@gmail.com

ABSTRACT

A logical basis for incorporating pressure non-equilibrium and turbulent eddy viscosity in an incompressible vortex model is presented. The infrasonic acoustic source implied in our earlier work has been examined. Finally, this non-equilibrium turbulent vortex core is shown to dissipate mechanical energy more slowly than a Burgers vortex, helping us to explain the persistence of axial vortices in nature. Recent molecular dynamics simulations replicate aspects of this non-equilibrium pressure behavior.

I. INTRODUCTION

Zuckerwar and Ash[1,2] have shown theoretically how fluids such as air and water can depart from thermodynamic equilibrium when subjected to intense local strain rates. Utilizing Hamilton's principle and quantifiable frequency-dependent acoustic parameters,[3] they were able to isolate thermodynamic non-equilibrium dilatational and shearing strain rate induced processes. We have shown previously how ambient weather conditions control dust devil and tornado core characteristics.[4] In Ref. 4 (Ash, Zuckerwar, and Zardadkhan[4] will be referred henceforth as AZZ), we examined strain rate driven departures from thermodynamic equilibrium in large-scale *incompressible* vortices, demonstrating the influence of relative humidity on the tornado core size and strength. This model evolved from the premise that extreme strain rates generated intense sound signatures while simultaneously forcing local fluid pressure to depart from thermodynamic equilibrium. Assuming quasi-reversible departures,[1,2] it was possible to develop a quantifiable *pressure relaxation coefficient*, controlled by ambient conditions. The pressure relaxation coefficient, η_p (measured in microseconds for air), is a measure of pressure gradient responsiveness.

In the 1960s, meteorologist Scorer proposed a hurricane and tornado formation process, whereby large-scale rotating air columns transformed suddenly from rotating cylinders to axial vortices.[5] Assuming mean angular momentum of the rotating parent was conserved, he avoided the nonphysical potential vortex centerline velocity limit by assuming the spontaneous potential vortex domain was annular. His finite cylindrical domain is consistent with observation, but he lacked a physically plausible mechanism to describe the creation of a Rankine vortex-like core region. He sketched a viscous core evolution process similar to a Lamb–Oseen vortex[6] evolution, but without providing details. Large-scale experimental verification of his model is lacking; only two small-scale experiments appear to support his postulated jump mechanism.[7,8] If the sudden inviscid transformation of a large-scale rotating column into a an inviscid axial vortex represents a natural jump instability process, the shearing strain rates imposed in the vicinity of the rotational axis most certainly reach unsustainable levels. If that is the case, away from the surface, the AZZ non-equilibrium pressure and azimuthal velocity model represents the resulting steady-state, circulation-controlled potential vortex. Furthermore, Scorer's finite outer radius limit bounds overall angular momentum and kinetic energy.

The AZZ non-equilibrium vortex study showed how unsustainable strain rates resulted when an inviscid axial vortex is imposed on a nominally incompressible fluid. Molecular dynamics simulations have exhibited a similar depressed kinetic energy-based pressure effect resulting from altered distributions of rotational degrees of freedom.[9] AZZ non-equilibrium theory predicted the following relations:

I. Far field circulation, Γ_∞, is twice the core circulation, i.e., if the maximum swirl velocity ($V_{\theta,Max}$) at core radius, R_{core}, is specified, $\Gamma_\infty = 4\pi R_{core} V_{\theta,Max}$.
II. For specified turbulent eddy viscosity, ν_{turb}, and pressure relaxation coefficient, η_p, the maximum swirl velocity is $V_{\theta,Max} = \sqrt{2\frac{\nu_{turb}}{\eta_p}}$.
III. If the maximum swirl velocity is known, the ratio of the turbulent eddy viscosity to the pressure relaxation coefficient can be estimated directly ($\frac{\nu_{turb}}{\eta_p} = \frac{V^2_{\theta,Max}}{2}$).
IV. The core radius is controlled by the imposed circulation and the inverse square root ratio of the turbulent eddy viscosity to the pressure relaxation coefficient, i.e., $R_{core} = \frac{\Gamma_\infty}{2^{5/2}\pi}\sqrt{\frac{\eta_p}{\nu_{turb}}}$.
V. The maximum out-of-equilibrium centerline pressure deficit is controlled by ambient density, ρ_∞, and the ratio of the turbulent eddy viscosity to the pressure relaxation coefficient, i.e., $\Delta P_{Min} = -4\rho_\infty \frac{\nu_{turb}}{\eta_p} \Rightarrow C_{p,Min} \equiv \frac{P(0)-P_\infty}{\frac{1}{2}\rho_\infty V^2_{\theta,Max}} = -4$.

In the absence of phase change energy release, buoyancy-induced rotating air columns become dust devil vortices rather than tornadoes. Large-scale dust devils are turbulent, but centrifugal forces suppress centerline fluctuations. Furthermore, Corrsin and Kistler[10] proved that when atmospheric turbulence is irrotational, mean velocity profiles are not influenced by that turbulence. The extreme shearing strain rates imposed near an inviscid vortex axis rule out thermodynamic equilibrium. Furthermore, near the core, sustainable imposed shearing strain rates organize atmospheric turbulence, producing local Reynolds stress gradients acting to resist that shear. On that basis, it was logical for AZZ to utilize the simple eddy viscosity turbulence model,

$$\sigma_{ij} = (\mu + \mu_{turb})\left[\frac{\partial v_i}{\partial x_j} + \frac{\partial v_j}{\partial x_i}\right] = \rho\nu_{turb}, \tag{1}$$

which only influences the steady-state vortex velocity field in the vicinity of the core. Sinclair[11] compiled the turbulent velocity, temperature, and pressure surveys for three dust devils with circulation levels between 320 m^2/s and 400 m^2/s. These data were employed in AZZ to develop the simple turbulent eddy viscosity correlation $\mu_{turb}/\mu = \nu_{turb}/\nu_{dryair} = 2.2 \pm 1$.

In our earlier study, we identified and partitioned an acoustic source approximation given by

$$\eta_p \frac{\partial}{\partial x_i}\left(\frac{DP}{Dt}\right) - \eta_p \frac{D}{Dt}\left(\frac{\partial P}{\partial x_i}\right) \approx \eta_p\left[\frac{\partial v_k}{\partial x_i}\frac{\partial P}{\partial x_k} - a_o^2 \frac{\partial}{\partial x_i}\left(\frac{D\rho}{Dt}\right)\right], \tag{2}$$

in which we found the local speed of sound, a_o, was accurate to three significant figures. Recently, a molecular dynamics simulation has isolated an analogous acoustic source in a small-scale hurricane-like simulation.[12] The two molecular dynamics simulations,[9,12] along with recent large-scale tornado simulator experiments reporting centerline pressure coefficient measurements as low as −2.8, beneath a boundary layer,[13] supporting the AZZ minimum $C_{p,Min} = -4$, away from any boundary layer influence, has motivated the present investigation. Unlike the compressible flow or water cavitation radial limits assumed historically to bound large-scale vortices in nature, we demonstrate a more fundamental incompressible vortex core departure from thermodynamic equilibrium prior to reaching those limits.

After validating the pressure relaxation coefficient, we have employed the AZZ acoustic source model along with turbulent eddy viscosity to examine the large-scale vortex core structure and associated infrasonic sound generation. Neglecting body forces, the AZZ incompressible non-equilibrium Navier–Stokes equation is

$$\rho\frac{D\mathbf{v}}{Dt} = -\nabla P + \eta_p \frac{D}{Dt}(\nabla \mathrm{P}) + \rho\nu_{turb}\nabla^2\mathbf{v}. \tag{3}$$

The steady-state, one-dimensional incompressible solutions $P(r)$, $v_\theta(r)$, have been utilized herein to test the usefulness of the AZZ model.

II. VALIDITY OF PRESSURE RELAXATION COEFFICIENT

Long-accepted quasi-reversible frequency-dependent sound attenuation models appear to violate the continuum *principle of coordinate invariance*. Normal shockwaves are irreversible, but continuum theory implies that both the shockwave thickness and frequency dependent sound attenuation are controlled by the second (or bulk) coefficient of viscosity. Thermodynamic equilibrium is assumed.

Zuckerwar and Meredith[14,15] have documented the process by which NASA reference-quality spectral acoustic absorption measurements are obtained (at frequencies between 10 Hz and 2500 Hz, in their case). Using these and similar data sources, estimates of the bulk viscosity of air are approximately three orders of magnitude larger than the dynamic viscosity—hardly justifying Stokes' negative second coefficient hypothesis. Furthermore, at moderate temperatures, the inferred bulk viscosity is influenced strongly by relative humidity.[3] The degree to which relative humidity influences experimentally measured bulk viscosity was our motivation for exploiting Hamilton's principle to incorporate non-equilibrium molecular (vibrational and rotational degrees of freedom) behavior in the conservation equations for air.[1,2]

Two non-equilibrium effects were identified: (1) a thermodynamic dilatational departure, indistinguishable from bulk viscosity, and (2) discovery that pressure could depart from thermodynamic equilibrium in otherwise incompressible flows.[1] Subsequently, we introduced multiple molecular degrees of freedom, showing how they could be incorporated in the non-equilibrium dilatational (volumetric) relaxation coefficient, η_V, and a similar *pressure relaxation coefficient*, η_P, defined strictly in terms of accepted acoustic parameters.[2] We showed that η_V, η_P-based shock thickness estimates over the Mach number range, $1 < M < 5$, agreed with the classical Boltzmann-equation-based estimates of Mott-Smith.[16] We also included the curious prediction that a non-equilibrium pressure effect occurred in incompressible slow viscous (Stokes) flow past a sphere.[2]

The pressure relaxation coefficient is based solely on standard acoustical reference parameters. Calculated pressure relaxation coefficients for dry and humid air in the 25 °C–40 °C temperature range were extremely small (less than 0.0001 s). However, as summarized in Table I, the pressure relaxation coefficient for dry air (0% RH) increases with increasing temperature, whereas the pressure relaxation coefficient for moisture saturated air (100% RH) decreases with increasing temperature. At moderate temperatures, the dry air

TABLE I. Influence of relative humidity on the pressure relation coefficient, η_p.

Ambient temperature (°C)	Pressure relaxation coefficient (RH = 0%) (s)	Pressure relaxation coefficient (RH = 100%)(s)	$\frac{\eta_{p,0\%}}{\eta_{p,100\%}}$
25	6.23×10^{-5}	2.16×10^{-7}	288
30	6.65×10^{-5}	1.83×10^{-7}	363
35	7.08×10^{-5}	1.55×10^{-7}	457
40	7.53×10^{-5}	1.32×10^{-7}	570

pressure relaxation coefficient is more than two orders of magnitude larger than 100% RH air. On that basis, it was logical to isolate pressure relaxation influences from turbulence in Eq. (3), when examining our non-equilibrium vortex model. AZZ theory predicts that the maximum swirl velocity is controlled by $\sqrt{2\frac{\nu_{turb}}{\eta_p}}$. At moderate tornado–hurricane-like ambient temperatures, the table shows that variations in relative humidity can increase or decrease maximum swirl velocity estimates by a factor of 10. *As the relative humidity increases, the pressure relaxation coefficient decreases, thus enabling atmospheric air to tolerate increased potential-flow-driven shearing strain rates, enhancing the circulation-driven vortex core strength.*

Testing the AZZ relations for tornadoes was more difficult. Not only are tornadoes much larger than dust devils, they are hazardous. Furthermore, tornadoes evolve randomly from strong interactions between fast-moving upper-level weather fronts and rising warm, moisture-laden air. Karstens *et al.*[17] have compiled *in situ* tornado pressure measurements for 26 tornadoes, dating from 1894. Starting in 2002, direct near-centerline pressure deficit measurements have been obtained. In six of the direct encounters, complimentary mobile mesonet data enable reasonably accurate estimates of ground level funnel width. Although actual ambient temperature and relative humidity conditions were uncertain, the six "near-direct" tornado encounters identified by Karstens *et al.* provided maximum pressure deficit and core radius data suitable for evaluating AZZ theory.

Without ambient and dewpoint temperatures (to determine tornado-based relative humidity), turbulence influences cannot be isolated from the pressure relaxation coefficient when employing only maximum pressure deficit measurements with associated core radius data.[17] However, humidity variations have only minor influences on ambient density, permitting reasonably accurate estimates of ρ_∞, based on ground track surface elevation and hour-by-hour weather service data. AZZ theory permits estimation of the maximum swirl velocity and far field circulation utilizing minimum pressure, core diameter, and ambient air density. The Tulia, TX tornado was of special interest because a fully instrumented SUV recorded the most extreme core pressure deficit (19 400 Pa) when it accidentally penetrated the tornado funnel. It has been difficult to explain how such an extreme pressure deficit could be produced due to violent vehicle motion within the core, but we assumed the measurement approximated the actual centerline pressure deficit. A summary of our estimates of maximum swirl velocity and far field circulation, based on the data from the work of Karstens *et al.*[17] (bold headings), along with ν_{tub}/η_p ratio estimates, is provided in Table II. Their pressure minimum and mesonet-based core radius measurements are in bold type. Estimated circulation levels are two orders of magnitude larger than Sinclair's dust devils.

TABLE II. Pressure deficits and core radii from Karstens *et al.*[17] along with AZZ estimates. Pressure minimum and mesonet-based core radius measurements are in bold type.

Tornado	ΔP_{Min} (Pa)	R_{core} (m)	$V_{\theta,Max}$ (m/s)	$\Gamma\infty$ (m^2/s)	ν_{tub}/η_p (m^2/s^2)
Mullinville, KS	**−2 200**	**265**	32.4	108 000	525
Manchester, SD #1	**−9 800**	**36**	68.4	31 000	2340
Manchester, SD #2	**−5 500**	**15**	51.2	9 600	1310
Webb, IA	**−2 700**	**54**	35.8	24 200	641
Tipton, KS	**−1 500**	**205**	26.8	69 000	359
Tulia, TX	**−19 400**	**30**	96.1	36 200	4620

III. A NON-EQUILIBRIUM SOLENOIDAL VORTEX

Saffman[18] showed that Burgers vortices[19] were one class of solenoidal vorticity solutions governed by

$$\frac{D\boldsymbol{\omega}}{Dt} = (\boldsymbol{\omega}\cdot\nabla)\boldsymbol{U} + \nu\nabla^2\boldsymbol{\omega} \tag{4}$$

when the mean velocity components were

$$U_i = \alpha_{ij}x_j, \text{ with } \alpha_{ii} = 0. \tag{5}$$

This vortex stretching mean velocity field stabilizes the Burgers vortex, avoiding the transient Lamb–Oseen vortex behavior.[6]

If a finite diameter Scorer potential vortex propels the flow, the imposed vorticity *is solenoidal*. The unsustainable circular non-equilibrium strain rate region around the rotational axis is the only departure from Saffman's $\boldsymbol{\omega} = \nabla\times\mathbf{V} = 0$. Utilizing the AZZ core radius and maximum swirl velocity to define reference circulation $\Gamma_\infty = 4\pi R_{core}V_{\theta,Max}$, the inviscid, Burgers,[19] and AZZ azimuthal velocity distributions can be represented,

$$v_{\theta,inviscid}(r) = 2V_{\theta,Max}\frac{1}{\left(\frac{r}{R_{core}}\right)}, \tag{6a}$$

$$v_{\theta,Burgers}(r) = 2V_{\theta,Max}\frac{1-e^{-\left(\frac{r}{R_{core}}\right)^2}}{\left(\frac{r}{R_{core}}\right)}, \tag{6b}$$

and

$$v_{\theta,AZZ}(r) = 2V_{\theta,Max}\frac{\frac{r}{R_{core}}}{1+\left(\frac{r}{R_{core}}\right)^2}, \tag{6c}$$

respectively. As shown in Fig. 1, the azimuthal Burgers vortex velocity profile approximates a potential vortex profile within two core radii, whereas the AZZ profile requires approximately five core radii to revert. The associated shearing rates of strain, given by

$$\dot{\varepsilon}_{r\theta}(r) = \frac{1}{2}\left[r\frac{\partial}{\partial r}\left(\frac{v_\theta}{r}\right) + \frac{1}{r}\frac{\partial v_r}{\partial\theta}\right] \to \frac{r}{2}\frac{d}{dr}\left(\frac{v_\theta}{r}\right), \tag{7}$$

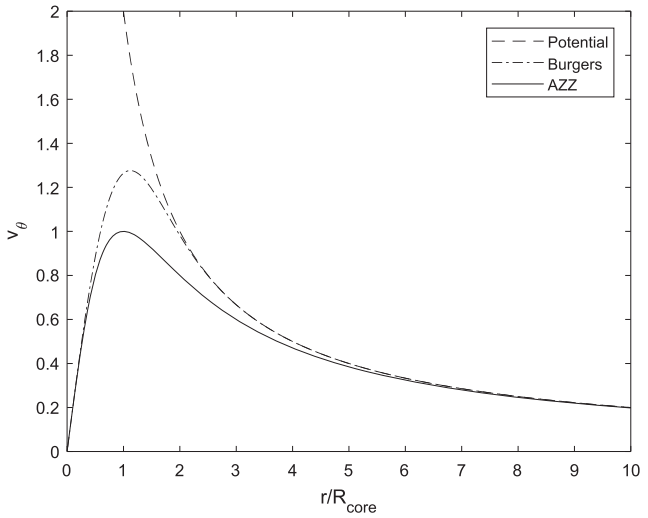

FIG. 1. Azimuthal velocity profiles for a potential vortex, a Burgers vortex, and a non-equilibrium AZZ vortex.

for Burgers and AZZ vortices are compared in Fig. 2. [The strain rate produced by a similarly scaled potential vortex is $\dot{\varepsilon}_{r\theta} = -2/(r/R_{core})^2$.] The AZZ strain rate relaxes more rapidly at first, and the magnitude of the most negative shearing strain rate is smaller than a Burgers vortex, approaching zero more rapidly thereafter.

Finally, the axial-vorticity-based dissipation function, ϵ, can be recast in a slightly different form in order to compare decay rates for a Burgers vortex with an AZZ vortex. That is,

$$\zeta_{Burgers}(r) = \frac{2V_{\theta,Max}R_{core}}{r}\frac{d}{dr}\left[1-\exp\left(-\frac{r^2}{R_{core}^2}\right)\right] = 4\frac{V_{\theta,Max}}{R_{core}}e^{-\left(\frac{r}{R_{core}}\right)^2} \tag{8}$$

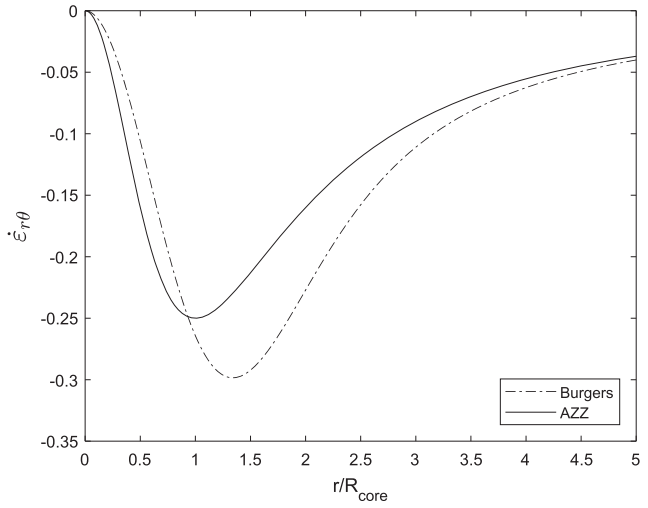

FIG. 2. Shearing strain rates produced by a Burgers vortex and a non-equilibrium AZZ vortex.

and

$$\zeta_{AZZ}(r) = \frac{2V_{\theta,Max}}{rR_{core}}\frac{d}{dr}\left[\frac{r^2}{1+\left(\frac{r}{R_{core}}\right)^2}\right] = 4\frac{V_{\theta,Max}}{R_{core}}\frac{1}{\left[1+\left(\frac{r}{R_{core}}\right)^2\right]^2}. \tag{9}$$

Thus,

$$\zeta^2_{Burgers}(r) = 16\left(\frac{V_{\theta,Max}}{R_{core}}\right)^2 e^{-2\left(\frac{r}{R_{core}}\right)^2}$$

and

$$\epsilon_{Burgers} = \rho\nu_{turb}\int_0^\infty 2\pi r\zeta^2(r)dr = 8\pi\rho\nu_{turb}V^2_{\theta,Max}. \tag{10}$$

The dissipation rate assuming a slowly decreasing maximum swirl velocity is compared with

$$\zeta^2_{AZZ}(r) = 16\left(\frac{V_{\theta,Max}}{R_{core}}\right)^2\frac{1}{\left[1+\left(\frac{r}{R_{core}}\right)^2\right]^4}$$

and

$$\epsilon_{AZZ} = \rho\nu_{turb}\int_0^\infty 2\pi r\zeta^2(r)dr = \frac{16\pi}{3}\rho\nu_{turb}V^2_{\theta,Max}. \tag{11}$$

The radial variation of *dissipation functions* $\left[\zeta^2(r/R_{core})\right]/\left[16\left(\frac{V_{\theta,Max}}{R_{core}}\right)^2\right]$ for a Burgers vortex and for an AZZ vortex is compared in Fig. 3. As shown in Fig. 3 and deduced from Eqs. (10) and (11), the mechanical energy dissipation rate in an AZZ vortex is smaller than a Burgers vortex. In fact, the mechanical rate of energy loss is only 2/3 that of a Burgers vortex. On that basis, a non-equilibrium axial vortex will be longer-lived than a Burgers vortex.

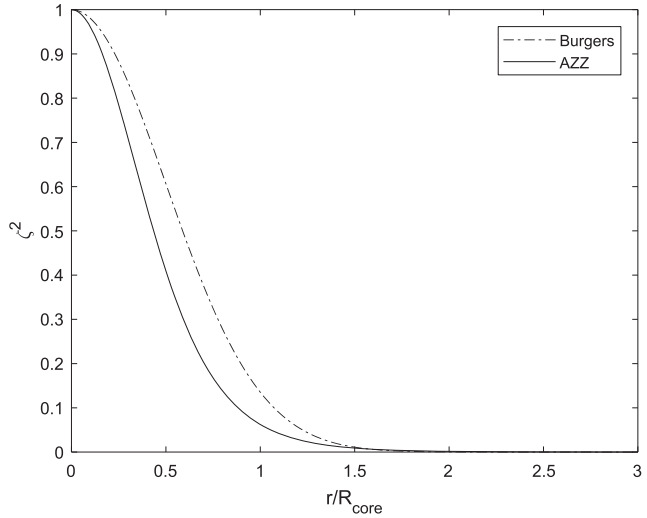

FIG. 3. Variation of dissipation functions $\zeta^2_{Burgers}\left(\frac{r}{R_{core}}\right)$ and $\zeta^2_{AZZ}\left(\frac{r}{R_{core}}\right)$, normalized with respect to $16\left(\frac{V_{\theta,Max}}{R_{core}}\right)^2$.

The Burgers vortex model[19] along with Saffman's generalization[18] and the Corrsin-Kistler turbulent mean velocity profile equivalence proof[10] has withstood the test of time. In the absence of Saffman's imposed three-dimensional mean velocity conditions, given by Eq. (5), the transient Burgers vortex reverts to the simple decay of a point or line vortex inserted suddenly in a viscous fluid.[6] Scorer's sudden transition of a large but finite diameter rotating cylindrical column with angular rotation rate, ω, into a finite circulation-imposed potential vortex ($\Gamma \approx \pi \frac{D_{Max}^2}{2}\omega$) creates unsustainable strain rates near the imposed axis. An equilibrium continuum flow model cannot tolerate such strain rates—in an otherwise incompressible flow. *The vortex core cannot be in thermodynamic equilibrium.*

IV. AN INFRASONIC GENERATION MECHANISM FOR LARGE-SCALE VORTICES

Triangulation of infrasonic storm signatures to locate severe tornado-capable weather has been an active area of research for some time.[20,21] If the maximum rotating column velocity (at R_{max}) is V_{column}, Scorer's inviscid transformation $v_\theta(r, t_{jump}) = \omega_{column} r \rightarrow \frac{\omega_{column} R_{max}^2}{r}$ for $0 \le r \le R_{max}$ produces unsustainable near-axis shearing strain rates during this rapid jump, radiating intense sound in the process. If the turbulent AZZ vortex results away from the surface, the mean velocity distribution becomes

$$\frac{\omega_{column} R_{max}^2}{r} \rightarrow v_\theta(r) = 2V_{\theta,MAX} \frac{\left(\frac{r}{R_{core}}\right)}{\left(\frac{r}{R_{core}}\right)^2 + 1} \tag{12}$$

with a rotating core whose angular rotation rate is

$$\omega_{core} = \frac{dv_\theta}{dr}(0) = 2\frac{V_{\theta,MAX}}{R_{core}} = 2\frac{\sqrt{2\frac{\nu_{turb}}{\eta_p}}}{\frac{\Gamma_\infty}{2^{5/2}\pi}\sqrt{\frac{\eta_p}{\nu_{turb}}}} = 16\frac{\pi}{\Gamma_\infty}\frac{\nu_{turb}}{\eta_p}. \tag{13}$$

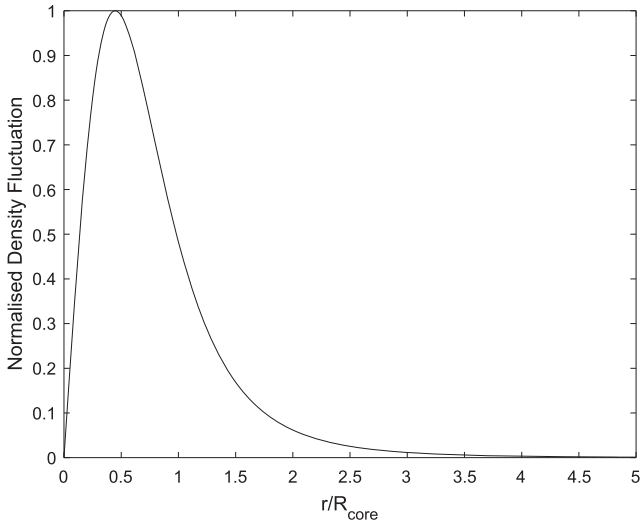

FIG. 4. Radial variation of acoustic density fluctuation. [Multiply by $-4\sqrt{5}\frac{V_{\theta,Max}^3}{a_o^2 R_{core}^2}$ to obtain 1/(s/m).]

The associated pressure distribution is

$$P(r) = P_\infty - \frac{\Delta P_{C/L}}{\left(\frac{r}{R_{core}}\right)^2 + 1} = P_\infty - 4\rho\frac{\nu_{turb}}{\eta_p}\frac{1}{(r/R_{core})^2 + 1}. \tag{14}$$

Employing Eqs. (12) and (14), the acoustic source, Eq. (2), can be represented,

$$\eta_p\left[\frac{\partial v_k}{\partial x_i}\frac{\partial P}{\partial x_k} - a_o^2\frac{\partial}{\partial x_i}\left(\frac{D\rho}{Dt}\right)\right]\boldsymbol{e}_i$$

$$\Rightarrow \left[\frac{\partial v_1}{\partial x_1}\frac{\partial P}{\partial x_1} + \frac{\partial v_2}{\partial x_1}\frac{\partial P}{\partial x_2}\right]\boldsymbol{e}_1 + \left[\frac{\partial v_1}{\partial x_2}\frac{\partial P}{\partial x_1} + \frac{\partial v_2}{\partial x_2}\frac{\partial P}{\partial x_2}\right]\boldsymbol{e}_2$$
$$= -a_o^2\left[\frac{\partial}{\partial x_1}\left(\frac{D\rho}{Dt}\right)\boldsymbol{e}_1 - \frac{\partial}{\partial x_2}\left(\frac{D\rho}{Dt}\right)\boldsymbol{e}_2\right]$$

or, in cylindrical coordinates,

$$\left[\frac{\partial v_k}{\partial x_i}\frac{\partial P}{\partial x_k}\right] \Leftrightarrow \begin{bmatrix} \frac{\partial v_r}{\partial r} & \left(\frac{1}{r}\frac{\partial v_r}{\partial \theta} - \frac{v_\theta}{r}\right) & \frac{\partial v_r}{\partial z} \\ \frac{\partial v_\theta}{\partial r} & \left(\frac{1}{r}\frac{\partial v_\theta}{\partial \theta} + \frac{v_r}{r}\right) & \frac{\partial v_\theta}{\partial z} \\ \frac{\partial v_z}{\partial r} & \frac{1}{r}\frac{\partial v_z}{\partial \theta} & \frac{\partial v_z}{\partial z} \end{bmatrix}\begin{bmatrix} \frac{\partial P}{\partial r} \\ \frac{1}{r}\frac{\partial P}{\partial \theta} \\ \frac{\partial P}{\partial z} \end{bmatrix}$$
$$= \begin{bmatrix} 0 & -\frac{v_\theta}{r} & 0 \\ \frac{dv_\theta}{dr} & 0 & 0 \\ 0 & 0 & 0 \end{bmatrix}\begin{bmatrix} \frac{dP}{dr} \\ 0 \\ 0 \end{bmatrix} = \begin{bmatrix} 0 \\ \frac{dv_\theta}{dr}\frac{dP}{dr} \\ 0 \end{bmatrix}.$$

The non-equilibrium rotating cylindrical volume creates a rotating acoustic source, given by

$$-4\boldsymbol{\rho}\frac{V_{\theta,Max}^3}{R_{core}^2}\frac{\frac{r}{R_{core}}}{\left[\left(\frac{r}{R_{core}}\right)^2 + 1\right]^3}\boldsymbol{e_\theta} = a_o^2\frac{\partial}{\partial r}\left(\frac{D\rho}{Dt}\right)\boldsymbol{e_\theta}. \tag{15}$$

In the swirling or azimuthal direction,

$$-4\frac{V_{\theta,Max}^3}{a_o^2 R_{core}^2}\frac{\frac{r}{R_{core}}}{\left[\left(\frac{r}{R_{core}}\right)^2 + 1\right]^3} = \frac{1}{\rho}\frac{\partial}{\partial r}\left(\frac{D\rho}{Dt}\right). \tag{16}$$

Hence, the density fluctuation magnitude is maximized at $r = \frac{R_{core}}{\sqrt{5}}$. That is,

$$\left|\frac{1}{\rho}\frac{\partial}{\partial r}\left(\frac{D\rho}{Dt}\right)\right|_{Max} = 4\sqrt{5}\frac{V_{\theta,Max}^3}{a_o^2 R_{core}^2}. \tag{17}$$

A normalized plot of the dimensionless variation of $\frac{1}{\rho}\frac{\partial}{\partial r}\left(\frac{D\rho}{Dt}\right)$ with (r/R_{core}) is shown in Fig. 4. Employing the Karstens data,[17] the minimum (largest magnitude) gradient of the material rate of change of density, normalized with respect to ambient density, varies from -3.4×10^{-5} 1/(s/m) to a much larger -0.075 1/(s/m) for the anomalous Tulia, TX tornado encounter. Additionally, a characteristic acoustic frequency produced by these rotating funnel cores should be related to the circulation-imposed centerline angular rotation rate, i.e., $\omega_{C/L} = 2V_{\theta,Max}/R_{core}$ or

$$f_{characteristic} = V_{\theta,Max}/(\pi R_{core}). \tag{18}$$

TABLE III. "Near direct" tornado data from the work of Karstens *et al.*[15]

Tornado	$\Delta \mathbf{P}_{\mathbf{Min}}$ (Pa)	$\mathbf{R}_{\mathbf{core}}$ (m)	$V_{\theta,Max}$ (m/s)	$\left[\frac{1}{\rho}\frac{\partial}{\partial r}\left(\frac{D\rho}{Dt}\right)\right]_{Min}$ (s/m)	Characteristic frequency (Hz)
Mullinville, KS	−2 200	265	32.4	-3.6×10^{-5}	0.04
Manchester, SD #1	−9 800	36	68.4	-1.8×10^{-2}	0.6
Manchester, SD #2	−5 500	15	51.2	-4.4×10^{-2}	1.0
Webb, IA	−2 700	54	35.8	-1.2×10^{-3}	0.2
Tipton, KS	−1 500	205	26.8	-3.4×10^{-5}	0.04
Tulia, TX	−19 400	30	96.1	−0.075	1.0

Dimensionless density fluctuation rates per unit height and characteristic frequencies for the six "near direct" tornado datasets are summarized in Table III. The estimated maximum swirl velocity of the Tulia, TX tornado assuming the unexplained extreme pressure deficit represents a border-line compressible flow condition ($M_{Tulia\ TX} = 0.275$). The Mach number represents a 3.7% ideal gas density decrease, i.e.,

$$\frac{\rho}{\rho_\infty} = \left[\frac{1}{1 + \frac{1.4-1}{2}(0.275)^2}\right]^{\frac{1}{1.4-1}} = 0.963. \tag{19}$$

which, when combined with the likely tumbling-vehicle-induced streamline distortions in such a non-equilibrium tornado core, may account for the substantially different $\left[\frac{1}{\rho}\frac{\partial}{\partial r}\left(\frac{D\rho}{Dt}\right)\right]_{Min}$. Hence, the AZZ acoustic density fluctuation estimates for the six documented tornado encounters appear reasonable.

V. CONCLUSIONS

Unlike man-made flow geometries where the shape and size of an object control the generation of vorticity and turbulence, characteristic scales of organized disturbances in the atmosphere can be much larger and a variety of large-scale swirling motions are observed without direct geometrical links to physical objects. In weather derived rotating systems, the transition from a rotating atmospheric column to a cyclone via spontaneous imposition of a line vortex is difficult to describe theoretically. Richard S. Scorer suggested that cyclonic transitions occurred when large, but finite, rotating atmospheric columns suddenly transformed morphologically into axial potential vortices, containing large but finite amounts of mechanical energy, conserving their angular momentum. We believe that large-scale rotating air columns when forced spontaneously to reform as potential vortices provide the mechanism by which cyclonic structures are generated. Unlike Scorer's proposal, we contend that the inner core structure is controlled by non-equilibrium pressure gradient forces generated by unsupportable shearing strain rates near the rotational axis. The resulting non-equilibrium AZZ vortex, just like the classical Burgers vortex, can be sustained by the vorticity stretching velocity conditions [Eq. (5)]. Furthermore, the non-equilibrium AZZ vortex dissipates mechanical energy more slowly and is therefore longer-lived.

ACKNOWLEDGMENTS

The first author would like to thank Dr. John H. Heinbockel for sharing his amazing applied mathematical insights and Dr. Joseph Werne for pointing out diplomatically that we had made a mathematical error in an early AZZ draft. This error isolated the acoustic generator mechanism described herein.

DATA AVAILABILITY

The data that support the findings of this study are available from the corresponding author upon reasonable request.

REFERENCES

[1] A. J. Zuckerwar and R. L. Ash, "Variational approach to the volume viscosity of fluid," Phys. Fluids **18**, 047101 (2006).
[2] A. J. Zuckerwar and R. L. Ash, "Volume viscosity in fluids with multiple dissipative processes," Phys. Fluids **21**, 033105 (2009).
[3] ANSI Standard S1, 26-1995, "Method for calculation of the absorption of sound by the atmosphere," Standards Secretariat of the Acoustical Society of America, New York, 1995.
[4] R. L. Ash, A. J. Zuckerwar, and I. R. Zardadkhan, "The influence of pressure relaxation on the structure of an axial vortex," Phys. Fluids **23**, 073101 (2011).
[5] R. S. Scorer, "Origin of cyclones," Sci. J. **2**, 46 (1966).
[6] C. W. Oseen, "Uber die wirbelbewegung in einer reibenden flusigkeit," Ark. Mat., Astron. Fys. **7**, 14 (1912).
[7] A. D. McEwan, "Angular momentum diffusion and the initiation of cyclones," Nature **260**, 126 (1976).
[8] S. C. Dickinson and R. R. Long, "Oscillating-grid turbulence including effects of rotation," J. Fluid Mech. **126**, 315 (1983).
[9] G. Meyer and G. Vitiello, "On the hurricane collective molecular dynamics," J. Phys.: Conf. Ser. **1275**, 012017 (2019).
[10] S. Corrsin and A. L. Kistler, "The free-stream boundaries of turbulent flow," NACA TR 1244, 1955.
[11] P. C. Sinclair, "The lower structure of dust devils," J. Atmos. Sci. **30**, 1599 (1969).
[12] K. H. Han, C. Kim, P. Talkner, G. E. Karniadakis, and E. K. Lee, "Molecular hydrodynamics: Vortex formation and sound wave propagation," J. Chem. Phys. **148**, 024506 (2018).
[13] Z. Tang, C. Feng, L. Wu, D. Zuo, and D. L. James, "Characteristics of tornado-like vortices simulated in a large-scale Ward-type simulator," Boundary-Layer Meteorol. **166**, 327 (2018).
[14] A. J. Zuckerwar and R. W. Meredith, "Low-frequency sound absorption measurements in air," NASA Reference Publication RP-1128, 1984.
[15] A. J. Zuckerwar and R. W. Meredith, "Low-frequency sound absorption measurements in air," J. Acoust. Soc. Am. **78**, 96 (1985).
[16] H. M. Mott-Smith, "The solution of the Boltzmann equation for a shock wave," Phys. Rev. **82**, 885 (1951).
[17] C. D. Karstens, T. M. Samaras, B. D. Lee, W. A. Gallus, Jr., and C. A. Finley, "Near-ground pressure and wind measurements in tornadoes," Mon. Weather Rev. **138**, 2570 (2010).
[18] P. G. Saffman, *Vortex Dynamics* (Cambridge University Press, Cambridge, 1992), p. 264.
[19] J. M. Burgers, "A mathematical model illustrating the theory of turbulence," Adv. Appl. Mech. **1**, 171 (1948).
[20] A. J. Abdullah, "The musical sound emitted by a tornado," Mon. Weather Rev. **94**, 213 (1966).
[21] B. R. Elbing, C. E. Petrin, and M. S. Van Den Broeke, "Measurement and characterization of infrasound from a tornado producing storm," J. Acoust. Soc. Am. **146**, 1528 (2019).